NATIONAL ADVISORY COMMITTEE FOR AERONAUTICS

TECHNICAL NOTE 2903

IMPINGEMENT OF CLOUD DROPLETS ON AERODYNAMIC BODIES AS AFFECTED BY COMPRESSIBILITY OF AIR FLOW AROUND THE BODY

By Rinaldo J. Brun, John S. Serafini, and Helen M. Gallagher

Lewis Flight Propulsion Laboratory
Cleveland, Ohio

Washington

March 1953

NATIONAL ADVISORY COMMITTEE FOR AERONAUTICS

TECHNICAL NOTE 2903

IMPINGEMENT OF CLOUD DROPLETS ON AERODYNAMIC BODIES AS AFFECTED BY COMPRESSIBILITY OF AIR FLOW AROUND THE BODY

By Rinaldo J. Brun, John S. Serafini, and Helen M. Gallagher

SUMMARY

The trajectories of water droplets in a compressible-air flow field around a cylinder were computed with a mechanical analog. The results of the calculations at approximately the flight critical Mach number were compared with calculations of trajectories in an incompressible flow field. For a cylinder, the effect of compressibility of the air on the droplet trajectories was negligible up to the flight critical Mach number. The results obtained with the cylinder were extended to airfoils. This extension is possible because the incompressible flow fields of both cylinders and airfoils are similarly altered by compressibility.

INTRODUCTION

The analytical study of ice formation on airfoils and other aerodynamic bodies exposed to icing clouds requires the calculation of the trajectories of the droplets with respect to the body. Previous investigators have calculated the water-droplet trajectories with respect to cylinders (references 1 to 3) and with respect to airfoils (references 4 to 6). All the calculations in the references cited were made with the assumption that the air surrounding the aerodynamic bodies behaved as an incompressible fluid. An evaluation of the effect of the compressibility of air in the flow field on the trajectories of cloud droplets is important, because many airfoils are now operated at high speed.

A knowledge of the air flow around the aerodynamic body is required in the calculations of the droplet trajectories, because the motion of a droplet is governed by the drag forces imposed on the droplet by its motion relative to the air moving along the air streamlines. The droplet momentum tends to keep the droplet moving in a straight path, while the drag forces tend to force the droplet to follow the streamlines.

Two-dimensional incompressible flow fields may be determined either from known mathematical relations or from electrolytic tank methods for most aerodynamic bodies. The compressible-air flow fields are extremely difficult to obtain for most aerodynamic bodies and are usually approximations or incompressible flow fields with corrections applied. A reasonably simple method for obtaining droplet-trajectory results in a compressible-air flow field is to evaluate the compressibility correction to be applied to trajectory data calculated for an incompressible flow field. Although the compressible-air flow field around a cylinder, which is obtained by applying correction terms to the incompressible flow field, is laborious to calculate, the cylinder flow field provides a relatively simple method for evaluating the correction required for compressibility.

In order to evaluate the magnitude of the compressibility effect on droplet impingement, trajectories in a compressible flow field around a cylinder were calculated at the NACA Lewis laboratory and the results compared with those of trajectories calculated in an incompressible flow field (reference 3). The compressible-air flow field was determined only for the cylinder flight critical Mach number, which is defined as that airspeed which results in sonic velocity at some location on the cylinder.

The results of the study of the effect of the compressibility of air around a cylinder are extended to include airfoils. The extension is based on a comparison of the compressible-air flow field around a cylinder at the cylinder flight critical Mach number with the compressible-air flow field around an airfoil at the airfoil critical Mach number.

SYMBOLS

The following symbols are used in this report:

a droplet radius, ft (3.048×10^5 microns)

C_D drag coefficient for droplets, dimensionless

E collection efficiency based on cylinder radius, dimensionless

K inertia parameter, $\frac{2}{9}\frac{\rho_w a^2 U}{\mu_0 L}$, dimensionless

L cylinder radius or airfoil chord length, ft

M Mach number, dimensionless

Re local Reynolds number with respect to droplet, $2a \rho_a \bar{v}/\mu$, dimensionless

Re_0 free-stream Reynolds number with respect to droplet, $2aU\left(\frac{\rho_a}{\mu}\right)_0$, dimensionless

r radial distance from cylinder axis to point in flow field, ratio to cylinder radius

t airfoil thickness, ratio to chord length

U free-stream velocity, ft/sec

u local air velocity, ratio of the actual velocity to the free-stream velocity

v local droplet velocity, ratio of actual velocity to free-stream velocity

$\bar{v}$ local vector difference between velocity of droplet and velocity of fluid, ft/sec

x,y rectangular coordinates, ratio of actual distance to cylinder radius L or airfoil chord length

α angle between x-axis and radial line to point in flow field, deg

γ ratio of specific heats

θ impingement angle on cylinder, deg

μ viscosity of air, slugs/(ft)(sec)

ρ density, slugs/cu ft

τ dimensionless time scale, ratio to time required for droplet to travel distance L at velocity U

φ $\frac{Re_0^2}{K} \equiv \frac{18LU}{\rho_w}\left(\frac{\rho_a^2}{\mu}\right)_0$, dimensionless

Subscripts:

a air

c compressible

i incompressible

m maximum

s surface

w water

x horizontal component

y vertical component

0 free stream

ANALYSIS

The differential equations that describe the motion of a droplet with respect to a cylinder have been derived in reference 3 and are presented here in the following form:

$$\frac{dv_x}{d\tau} = \frac{C_D Re}{24} \frac{1}{K} (u_x - v_x)$$

$$\frac{dv_y}{d\tau} = \frac{C_D Re}{24} \frac{1}{K} (u_y - v_y) \tag{1}$$

where

$$K \equiv \frac{2}{9} \frac{\rho_w a^2 U}{\mu_0 L} \tag{2}$$

and the Reynolds number Re can be obtained conveniently in terms of the free-stream Reynolds number

$$Re_0 = 2aU \left(\frac{\rho_a}{\mu}\right)_0 \tag{3}$$

such that

$$\left(\frac{Re}{Re_0}\right)^2 = \left(\frac{\rho_a}{\rho_{a,0}} \frac{\mu_0}{\mu}\right)^2 \left[(u_x - v_x)^2 + (u_y - v_y)^2\right] \tag{4}$$

The differential equations (1) state that the motion of a droplet is governed by the drag forces imposed on the droplet by virtue of the relative velocities between the droplet and the local air in motion along the streamlines around the cylinder. The compressible-air flow around a right circular cylinder of infinite extent is described by the following equations:

$$
\begin{aligned}
u_x = {} & \left[(1 - r^{-2})\cos^2\alpha + (1 + r^{-2})\sin^2\alpha\right] + \\
& M^2\left[\left(-\frac{13}{12}r^{-2} + \frac{3}{2}r^{-4} - \frac{5}{12}r^{-6}\right)\cos^2\alpha + \left(\frac{1}{4}r^{-2} - \frac{1}{4}r^{-4}\right)\cos\alpha\cos 3\alpha - \right. \\
& \left.\left(-\frac{13}{12}r^{-2} + \frac{1}{2}r^{-4} - \frac{1}{12}r^{-6}\right)\sin^2\alpha - \left(\frac{3}{4}r^{-2} - \frac{1}{4}r^{-4}\right)\sin\alpha\sin 3\alpha\right] + \\
& M^4\left\{(\gamma-1)\left[\left(-\frac{17}{60}r^{-2} + \frac{3}{8}r^{-4} - \frac{5}{12}r^{-6} + \frac{7}{16}r^{-8} - \frac{9}{80}r^{-10}\right)\cos^2\alpha + \right.\right. \\
& \left(+\frac{61}{80}r^{-4} - \frac{15}{16}r^{-6} + \frac{7}{40}r^{-8}\right)\cos\alpha\cos 3\alpha + \left(-\frac{3}{16}r^{-4} + \frac{3}{16}r^{-6}\right)\cos\alpha\cos 5\alpha\Big] + \\
& \left[\left(-\frac{137}{80}r^{-2} + 4\,r^{-4} - \frac{65}{16}r^{-6} + \frac{35}{16}r^{-8} - \frac{33}{80}r^{-10}\right)\cos^2\alpha + \right. \\
& \left(+\frac{19}{48}r^{-2} + \frac{5}{16}r^{-4} - \frac{15}{16}r^{-6} + \frac{7}{24}r^{-8} - \frac{1}{16}r^{-10}\right)\cos\alpha\cos 3\alpha + \\
& \left.\left(-\frac{1}{16}r^{-2} - \frac{3}{16}r^{-4} + \frac{1}{4}r^{-6}\right)\cos\alpha\cos 5\alpha\right] - \\
& (\gamma-1)\left[\left(-\frac{17}{60}r^{-2} + \frac{1}{8}r^{-4} - \frac{1}{12}r^{-6} + \frac{1}{16}r^{-8} - \frac{1}{80}r^{-10}\right)\sin^2\alpha + \right. \\
& \left(\frac{61}{80}r^{-4} - \frac{9}{16}r^{-6} + \frac{3}{40}r^{-8}\right)\sin\alpha\sin 3\alpha + \left(-\frac{5}{16}r^{-4} + \frac{3}{16}r^{-6}\right)\sin\alpha\sin 5\alpha\Big] - \\
& \left[\left(-\frac{137}{80}r^{-2} + \frac{4}{3}r^{-4} - \frac{13}{16}r^{-6} + \frac{5}{16}r^{-8} - \frac{11}{240}r^{-10}\right)\sin^2\alpha + \right. \\
& \left(\frac{19}{16}r^{-2} + \frac{5}{16}r^{-4} - \frac{9}{16}r^{-6} + \frac{1}{8}r^{-8} - \frac{1}{48}r^{-10}\right)\sin\alpha\sin 3\alpha + \\
& \left.\left.\left.\left(-\frac{5}{16}r^{-2} - \frac{5}{16}r^{-4} + \frac{1}{4}r^{-6}\right)\sin\alpha\sin 5\alpha\right]\right\}
\end{aligned}
\tag{5a}
$$

and

$$
\begin{aligned}
u_y = {} & \left[-r^{-2} \sin 2\alpha\right] + \\
& M^2 \left[\left(-\frac{13}{12} r^{-2} + \frac{3}{2} r^{-4} - \frac{5}{12} r^{-6}\right) \sin\alpha\cos\alpha + \left(\frac{1}{4} r^{-2} - \frac{1}{4} r^{-4}\right) \sin\alpha\cos 3\alpha + \right. \\
& \left.\left(-\frac{13}{12} r^{-2} + \frac{1}{2} r^{-4} - \frac{1}{12} r^{-6}\right) \sin\alpha\cos\alpha + \left(\frac{3}{4} r^{-2} - \frac{1}{4} r^{-4}\right) \cos\alpha\sin 3\alpha\right] + \\
& M^4 \left\{(\gamma-1) \left[\left(-\frac{17}{60} r^{-2} + \frac{3}{8} r^{-4} - \frac{5}{12} r^{-6} + \frac{7}{16} r^{-8} - \frac{9}{80} r^{-10}\right) \sin\alpha\cos\alpha + \right.\right. \\
& \left(\frac{61}{80} r^{-4} - \frac{15}{16} r^{-6} + \frac{7}{40} r^{-8}\right) \sin\alpha\cos 3\alpha + \left(-\frac{3}{16} r^{-4} + \frac{3}{16} r^{-6}\right) \sin\alpha\cos 5\alpha\Big] + \\
& \left[\left(-\frac{137}{80} r^{-2} + 4 r^{-4} - \frac{65}{16} r^{-6} + \frac{35}{16} r^{-8} - \frac{33}{80} r^{-10}\right) \sin\alpha\cos\alpha + \right. \\
& \left(\frac{19}{48} r^{-2} + \frac{5}{16} r^{-4} - \frac{15}{16} r^{-6} + \frac{7}{24} r^{-8} - \frac{1}{16} r^{-10}\right) \sin\alpha\cos 3\alpha + \\
& \left.\left(-\frac{1}{16} r^{-2} - \frac{3}{16} r^{-4} + \frac{1}{4} r^{-6}\right) \sin\alpha\cos 5\alpha\right] + \\
& \left[\left(-\frac{137}{80} r^{-2} + 4 r^{-4} - \frac{65}{16} r^{-6} + \frac{35}{16} r^{-8} - \frac{33}{80} r^{-10}\right) \sin\alpha\cos\alpha + \right. \\
& \left(\frac{19}{48} r^{-2} + \frac{5}{16} r^{-4} - \frac{15}{16} r^{-6} + \frac{7}{24} r^{-8} - \frac{1}{16} r^{-10}\right) \sin\alpha\cos 3\alpha + \\
& \left.\left(-\frac{1}{16} r^{-2} - \frac{3}{16} r^{-4} + \frac{1}{4} r^{-6}\right) \sin\alpha\cos 5\alpha\right] + \\
& (\gamma-1) \left[\left(-\frac{17}{16} r^{-2} + \frac{1}{8} r^{-4} - \frac{1}{12} r^{-6} + \frac{1}{16} r^{-8} - \frac{1}{80} r^{-10}\right) \sin\alpha\cos\alpha + \right. \\
& \left(\frac{61}{80} r^{-4} - \frac{9}{16} r^{-6} + \frac{3}{40} r^{-8}\right) \sin 3\alpha\cos\alpha + \left(-\frac{5}{16} r^{-4} + \frac{3}{16} r^{-6}\right) \sin 5\alpha\cos\alpha\Big] + \\
& \left[\left(-\frac{137}{80} r^{-2} + \frac{4}{3} r^{-4} - \frac{13}{16} r^{-6} + \frac{5}{16} r^{-8} - \frac{11}{240} r^{-10}\right) \sin\alpha\cos\alpha + \right. \\
& \left(\frac{19}{16} r^{-2} + \frac{5}{16} r^{-4} - \frac{9}{16} r^{-6} + \frac{1}{8} r^{-8} - \frac{1}{48} r^{-10}\right) \sin 3\alpha\cos\alpha + \\
& \left.\left.\left.\left(-\frac{5}{16} r^{-2} - \frac{5}{16} r^{-4} + \frac{1}{4} r^{-6}\right) \sin 5\alpha\cos\alpha\right]\right\}
\end{aligned}
\tag{5b}
$$

The first bracketed term describes the incompressible flow around the cylinder. The term with the M^2 factor and the term with the M^4 factor are, respectively, the first- and second-order corrections for the effect of compressibility on the incompressible flow field. The expression for the velocity potential, from which equations (5a) and (5b) were derived, was obtained from reference 7. In equation (5), α is measured counterclockwise from the x-axis of the cylinder, as is shown in figure 1.

Equations (1) to (5) are written in dimensionless form in order to maintain the number of calculations to a minimum and to simplify the presentation of the results. The equations apply to the motion of droplets in a plane perpendicular to the axis of the cylinder, which is located at the origin of the coordinate system (fig. 1). At an infinite distance ahead of the cylinder the uniform air flow carrying the cloud droplets is assumed to be approaching the cylinder from the negative x-direction and parallel to the x-axis. All the distances appearing in the equations are ratios to the cylinder radius L, which is assumed to be the unit of distance. The velocities appear as fractional parts of the free-stream velocity U. Time is expressed in terms of the cylinder radius and free-stream velocity such that the unit of time is the time required for a droplet to travel a distance L at velocity U.

The more important assumptions that have been necessary in order to solve the problems are:

(1) At a large distance ahead of the airfoil (free-stream conditions) the droplets move with the same velocity as the air.

(2) The droplets are always spherical and do not change in size.

(3) No gravitational force acts on the droplets.

(4) The ratio of the local viscosity μ to the free-stream viscosity μ_0, appearing in equation (4), is unity. This assumption is valid, because viscosity is not appreciably affected by the order of magnitude of the changes in temperature found along a trajectory.

METHOD OF CALCULATION

The nonlinear differential equations of motion (equations (1)) are difficult to solve by ordinary means, because the velocity components of the air and the term containing the coefficient of drag are variable at all points in the flow field and cannot be related in closed form. Simultaneous solutions for the two equations were obtained with a mechanical analog based on the principle of a differential analyzer (reference 3). The answers were obtained in the form of plots of the droplet trajectories with respect to the cylinder, as shown in figure 2.

The second-quadrant section of the cylinder is outlined in figure 2. As is shown in the figure, the ordinate scale was expanded approximately four times the abscissa scale in the mechanical analog in order to gain accuracy in determining the points of impingement of the droplets on the cylinder surface. The droplets were assumed to start at an infinite distance ahead of the cylinder at an initial ordinate of y_0 (fig. 1), but only the last 5 radii of distance in the x-direction were plotted by the machine. The starting conditions at $x = -5$ were obtained by use of equations described in references 2 and 3. The reference angle θ in figure 2 is measured clockwise from the negative x-axis of the cylinder.

Trajectories, such as those shown in figure 2, computed for several combinations of values of K and Re_0 permit the evaluation of the amount and extent of water-droplet impingement on cylinders. The cylinder data are presented herein in terms of the dimensionless parameters K and φ used in reference 3. The parameter K (equation (2)) has been termed the inertia parameter because its magnitude directly reflects the external force required on a droplet to cause a deviation from the original line of motion of the droplet. The dimensionless parameter φ is defined

$$\varphi \equiv \frac{Re_0^2}{K} = \frac{18LU}{\rho_w}\left(\frac{\rho_a^2}{\mu}\right)_0 \tag{6}$$

The magnitude of φ is a measure of the deviation from Stokes' law for the forces acting on the water droplets. Stokes' law was derived for slow translatory motion of a small sphere in an incompressible viscous fluid and applies precisely in the limiting value of $\varphi = 0$.

The parameters K and φ together are sufficient to define the conditions of a particular impinging droplet. Because of the nature of the dimensionless parameters, an infinite number of combinations of values of the variables, such as free-stream velocity, cylinder size, droplet size, and others (equations (2), (3), and (6)), would apply to the particular value of the dimensionless parameter under consideration. A system of equations for the evaluation of dimensionless parameters in terms of variables with units commonly employed in aeronautics is presented in appendix C of reference 3.

The compressible-air velocity components in the flow field (equations (5)) were calculated at a Mach number of 0.4, because the effect of compressibility for completely subsonic flow is considered greatest at or near the flight critical Mach number. The value obtained for the flight critical Mach number depends on the number of correction terms applied to the incompressible flow field and appears to approach 0.4 as

a limit. This value of Mach number corresponds to a speed of approximately 290 miles per hour at an altitude of 10,000 feet. Results presented herein involve the maximum effect of compressibility, which restricts the free-stream velocity to a value compatible with a Mach number of 0.4.

Because of the difficulties in making precise corrections to the coefficient-of-drag term in equations (1) and to the density terms in equation (4), the problem was solved in two steps. The first step was to survey a range of values of the parameters K and φ to determine the conditions most affected by compressibility. For this survey the term $C_D Re/24$, containing the coefficient of drag for the droplets, required in equations (1), was assumed to be a function of the local Reynolds number Re only and not related to the Mach number. The values for $C_D Re/24$ were obtained from tables in reference 2. Also, the density ratio appearing in equation (4) was assumed to be unity for this survey. The second step was to apply first-order corrections to the coefficient-of-drag term and to equation (4) for density variations along the particular trajectory that showed the largest effect caused by the compressible-air flow field. The difference in the trajectories caused by the correction was less than the probable error of the analog.

RESULTS AND DISCUSSION

Presentation of Results

The solid lines in figure 2 are the trajectories for droplets in a compressible-air flow field calculated at the flight critical Mach number for the cylinder ($M_0 = 0.4$), and the dashed lines are the trajectories for droplets in an incompressible flow field. The set of lines labeled A are trajectories of droplets with large momentum, that is, large in size and moving with high speed. The momentum of these droplets is so large that the trajectories are nearly straight lines. One combination of operating conditions for which the trajectories labeled A would be applicable involves a cylinder 1/2 inch in diameter moving with a free-stream velocity of 290 miles per hour through a cloud composed of uniform droplets approximately 26 microns in diameter at a 10,000-foot altitude. The trajectories labeled A are tangent to the cylinder at the point of interception. All droplets with the same values of parameters K and φ having trajectories below these trajectories strike the cylinder; whereas, all droplets with the same values of φ and K having trajectories above these lines will miss the cylinder. The initial ordinate y_0 of the droplets at $x = -\infty$ (fig. 1) is given in figure 2.

A comparison of the trajectories computed for the compressible-air flow field with those for an incompressible flow field shows that for

droplets with large values of the inertia parameter K (trajectories A, fig. 2) the effect of compressibility is imperceptible. The effect of compressibility is also negligible on trajectories of droplets with low values of K, as shown by the set of tangent trajectories labeled B. These trajectories would apply, for example, to a cylinder 1 inch in diameter moving with a free-stream velocity of 290 miles per hour through a cloud composed of uniform droplets approximately 4 microns in diameter at a 10,000-foot altitude.

The greatest effect of compressibility on tangent trajectories is found in the middle range of the droplet inertia parameter K, as shown by the set of trajectories labeled C in figure 2. Both trajectories are tangent to the cylinder, but the droplets had to start at different ordinates in order to arrive tangent. For the droplets having trajectories labeled C, the collection efficiency ($E_m = y_{0,m}$), defined as the ratio of the actual water impinging on the cylinder to the total water in the volume swept out of its path by the cylinder, is 0.501 if compressibility is accounted for, as compared with 0.514 when compressibility is ignored.

The collection efficiency E_m for a cylinder in a compressible-air flow field at approximately the flight critical Mach number ($M_0 = 0.4$) is presented in figure 3 as a function of inertia parameter K and dimensionless parameter φ.

The effect of compressibility on the collection efficiency is shown in figure 4 as a percent difference. The difference is obtained from the relation

$$\text{percent difference} = \frac{E_{m,i} - E_{m,c}}{E_{m,c}} (100)$$

where the values for $E_{m,i}$ are obtained from the collection efficiency presented in reference 3 for the incompressible flow field. The greatest difference is about 3 percent at the conditions of $K = 5$ and $\varphi = 50{,}000$. The following tabulation summarizes the effect of compressibility as a percent difference between results computed in a compressible and an incompressible flow field. Typical values of dimensions and flight conditions are involved in the examples given. All calculations were made for 290 miles per hour, which is near the critical speed for cylinders at the 10,000-foot NACA standard altitude.

Inertia parameter K	Cylinder diameter D (in.)	Droplet diameter d (microns)	Dimensionless parameter φ	$\frac{E_{m,i} - E_{m,c}}{E_{m,c}}(100)$ (percent)
0.5	1/2	3	740	0.3
.5	1	4	1,480	.4
.5	3	7	4,440	.5
.5	6	9	8,880	.5
1	1/2	4	740	.6
1	1	5	1,480	.8
1	3	9	4,440	.9
1	6	13	8,880	1.0
5	1/2	9	740	1.5
5	1	12	1,480	1.9
5	3	21	4,440	2.1
5	6	30	8,880	2.3
5	18	50	27,650	2.8
5	30	70	44,400	2.9
20	1/2	17	740	.5
20	1	24	1,480	.6
20	3	40	4,440	.7
20	6	60	8,880	.8

Discussion of Results

From the results of the tabulation and of figure 4, it may be concluded that for a cylinder the effect of compressibility of the air on the droplet trajectories is not very great up to the flight critical Mach number; and for most practical problems involving measurements of droplet impingement on cylinders, the compressibility effect may be ignored.

The reason that the effect of compressibility on droplet trajectories is nearly negligible is found in the comparison of the compressible-air flow field with the incompressible flow field. The effect of compressibility is most pronounced on those streamlines close to the cylinder. The compressibility effect decreases very rapidly with distance away from the surface of the cylinder and everywhere becomes negligible 1 cylinder radius away from the surface. Furthermore, the effect of compressibility is of consequence only over the top portion of the cylinder, as shown in figure 5. The comparison between the compressible and incompressible tangential air-flow velocities on the cylinder surface (fig. 5) shows that the effect is pronounced only for $\theta > 60^{\circ}$. The angle is measured from the same reference line as in figure 1.

Droplets forming the solid-line trajectory labeled A in figure 2 are acted on, during the last portion of the trajectory, by air streamlines that have a different pattern from the air streamlines for an incompressible flow field; however, the inertia of these droplets is so large that the last portion of their path is not influenced appreciably by the compressibility of the air flow. The droplets with low inertia (trajectories labeled B, fig. 2) are always in the flow-field region where there is no appreciable difference between the compressible and incompressible air flows. The droplets in the middle range of inertia have the last portion of the trajectories in a region where the effect of compressibility on the air flow is of some consequence. The inertia of these droplets is low enough to be influenced. Droplets with trajectories labeled D and E have the same middle range of inertia as those with trajectories C. Trajectories D and E are not influenced by compressibility for the same reason that trajectory B was not influenced.

The sample trajectories presented in figure 2 summarize the effect of compressibility over the complete range of values studied for the parameters K and φ. The small effect of compressibility is most pronounced on collection efficiency (figs. 3 and 4). The effect on the maximum angle of impingement θ_m was within the accuracy of the analog. The effect on trajectories intermediate between the tangent trajectory and the x-axis is imperceptible (trajectories D and E, fig. 2). For this reason, the values of the local rate of impingement (the term β in reference 3) are not affected by compressibility.

Extension of Cylinder Results to Airfoils

The extension of the results obtained with a cylinder to an airfoil is justifiable, because the incompressible flow fields of cylinders and airfoils are similarly altered by compressibility. A comparison between the compressible and incompressible velocities on the surfaces of two symmetrical Joukowski airfoils is shown in figure 6. The curves of figure 6 were obtained from results presented in reference 8. The ratio of the surface velocity to the free-stream velocity is plotted as a function of the chordwise station, given as a ratio to the chord length. The results of figure 6 indicate that the effect of compressibility becomes less pronounced as the thickness ratio t of the airfoil is decreased and the critical Mach number is increased.

As was found for the cylinder, the greatest effect of compressibility is in the vicinity of the thickest part of the airfoil. Analysis based on the work presented in references 5 and 6 indicates that under normal icing conditions the impingement occurs on the nose section of the airfoil. As with the cylinder, the nose section is not affected to a significant degree by compressibility. Those droplets that impinge on the

thick part of the airfoil have such large inertia that small differences in air-flow velocity components close to the airfoil do not appreciably affect their trajectories.

Aerodynamic considerations show that the superposition of circulation on the air-flow field, as would be caused by placing the airfoil at an angle of attack, would tend to cause a shift in the location of the maximum difference between the compressible and incompressible air flows. The circulation would shift the maximum difference toward the nose on the top surface and toward the tail on the bottom surface, because circulation increases the air velocity around the top surface, especially near the nose, and decreases the velocity near the bottom surface. However, a change in angle of attack also causes a shift in the area of impingement in the same direction, that is, toward the nose on the top surface and toward the tail on the bottom surface; therefore, the area of impingement would probably remain in the region where the effect of compressibility is of no practical consequence.

The curves of figure 6 are for Joukowski airfoils, which are more blunt-nosed than modern high-speed airfoils. The chordwise location of the maximum velocity occurs at approximately $x = 0.1$ for the Joukowski airfoil; whereas, the chordwise location of the maximum velocity occurs from $x = 0.3$ to $x = 0.5$ on high-speed airfoils, depending on the design lift coefficient. The area of droplet impingement, however, is at the nose section for a high-speed airfoil (reference 6), as in the case of the Joukowski airfoil (reference 5). The arguments used in concluding that the effect of the compressibility of air is negligible on droplet trajectories impinging on a Joukowski airfoil, for which the flow field is a direct transformation from a cylinder, are applicable to modern high-speed airfoils, because the air-flow regions with the greatest compressibility of the air occur on the airfoil well back of the regions of droplet impingement.

CONCLUSIONS

The following conclusions are based on the calculation of droplet trajectories around a cylinder in both an incompressible flow field and a compressible-air flow field at the flight critical Mach number and on a study of the air velocities around airfoils:

1. For a cylinder the effect of compressibility of the air on the droplet trajectories is not very great up to the flight critical Mach number, and for most practical problems involving measurements of droplet impingement on cylinders the compressibility effect may be ignored.

2. The fact that the effect of compressibility on the impinging droplet trajectories is negligible also applies to airfoils.

Lewis Flight Propulsion Laboratory
National Advisory Committee for Aeronautics
Cleveland, Ohio, September 11, 1952

REFERENCES

1. Glauert, Muriel: A Method of Constructing the Paths of Raindrops of Different Diameters Moving in the Neighborhood of (1) a Circular Cylinder, (2) an Aerofoil, Placed in a Uniform Stream of Air; and a Determination of the Rate of Deposit of the Drops on the Surface and the Percentage of Drops Caught. R. & M. No. 2025, British A.R.C., 1940.

2. Langmuir, Irving, and Blodgett, Katherine B.: A Mathematical Investigation of Water Droplet Trajectories. Tech. Rep. No. 5418, Air Materiel Command, AAF, Feb. 19, 1946. (Contract No. W-33-038-ac-9151 with General Electric Co.)

3. Brun, Rinaldo J., and Mergler, Harry W.: Impingement of Water Droplets on a Cylinder in an Incompressible Flow Field and Evaluation of Rotating Multicylinder Method for Measurement of Droplet-Size Distribution, Volume-Median Droplet Size, and Liquid-Water Content in Clouds. NACA TN 2904, 1953.

4. Bergrun, Norman R.: A Method for Numerically Calculating the Area and Distribution of Water Impingement on the Leading Edge of an Airfoil in a Cloud. NACA TN 1397, 1947.

5. Guibert, A. G., Janssen, E., and Robbins, W. M.: Determination of Rate, Area, and Distribution of Impingement of Waterdrops on Various Airfoils from Trajectories Obtained on the Differential Analyzer. NACA RM 9A05, 1949.

6. Brun, Rinaldo J., Serafini, John S., and Moshos, George J.: Impingement of Water Droplets on an NACA 65_1-212 Airfoil at an Angle of Attack of 4°. NACA RM E52B12, 1952.

7. Eser, F. (M. Flint, Trans.): On the Flow of Compressible Fluids Past Solid Bodies at Subsonic Velocity. Luftfahrtforschung, vol. 20, no. 7, July 20, 1943, pp. 220-230. R.T.P. Translation No. 2056, Ministry Aircraft Prod. (British).

8. Kaplan, Carl: Compressible Flow about Symmetrical Joukowski Profiles. NACA Rep. 621, 1938.

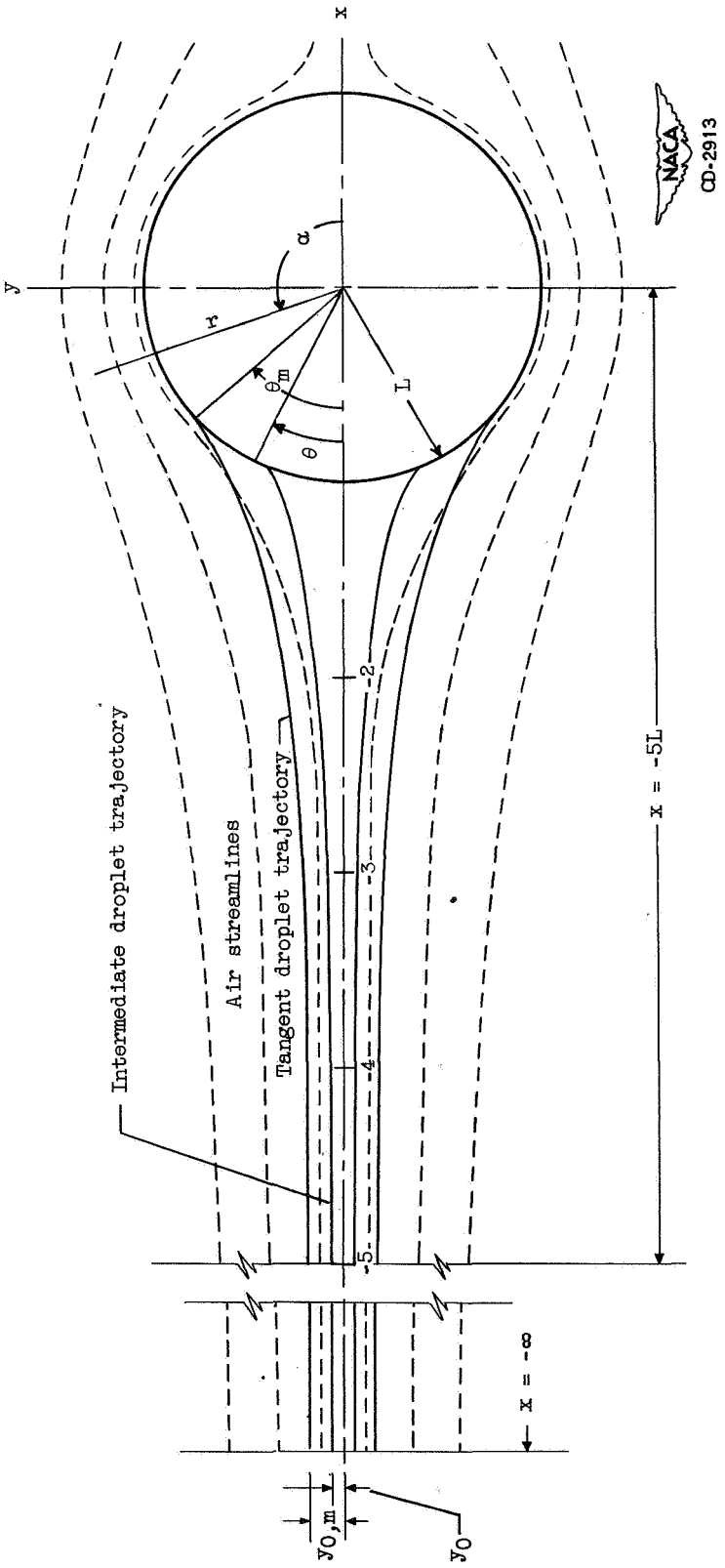

Figure 1. - Coordinate system for cylinder.

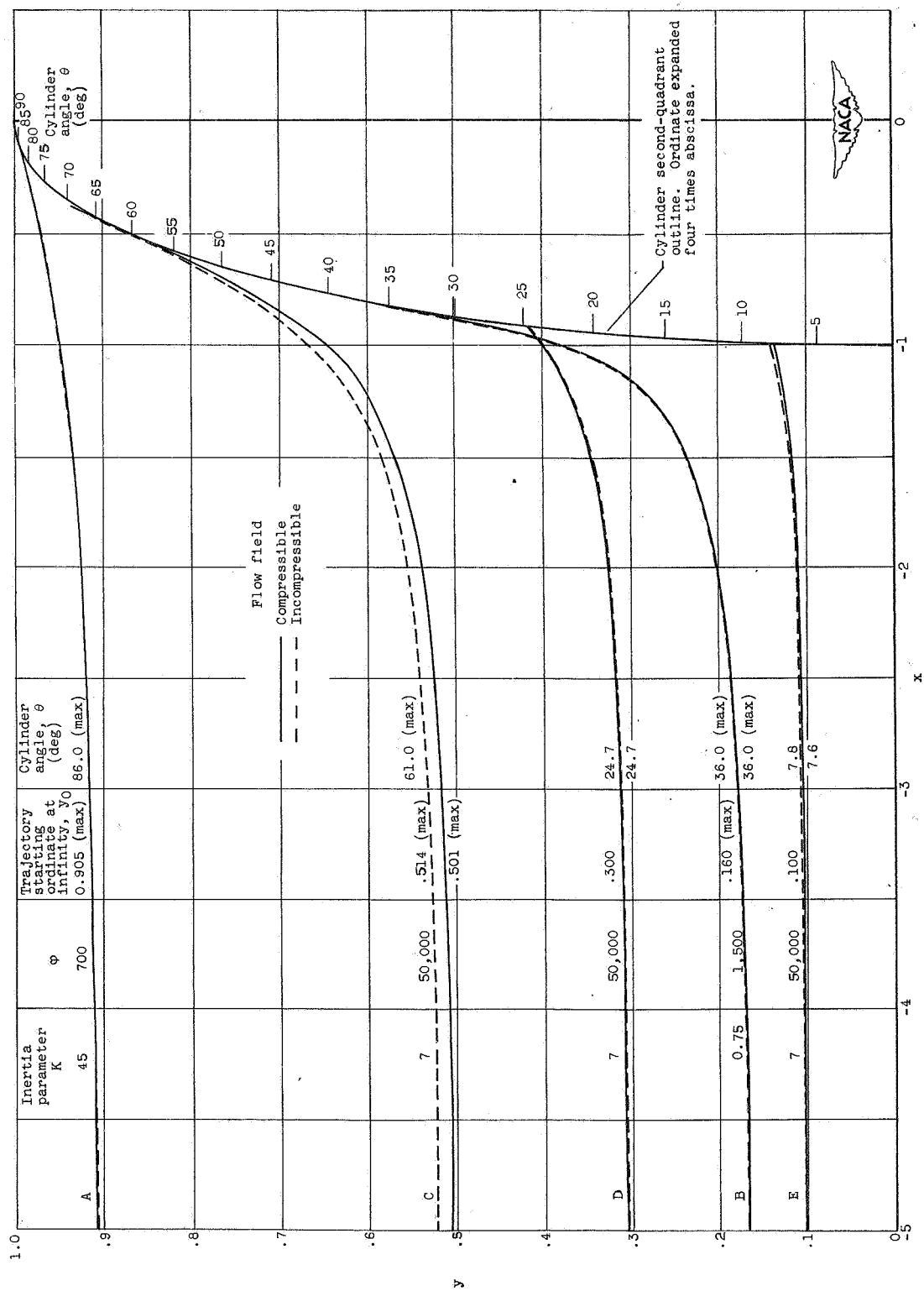

Figure 2. - Trajectories of droplets impinging on a cylinder.

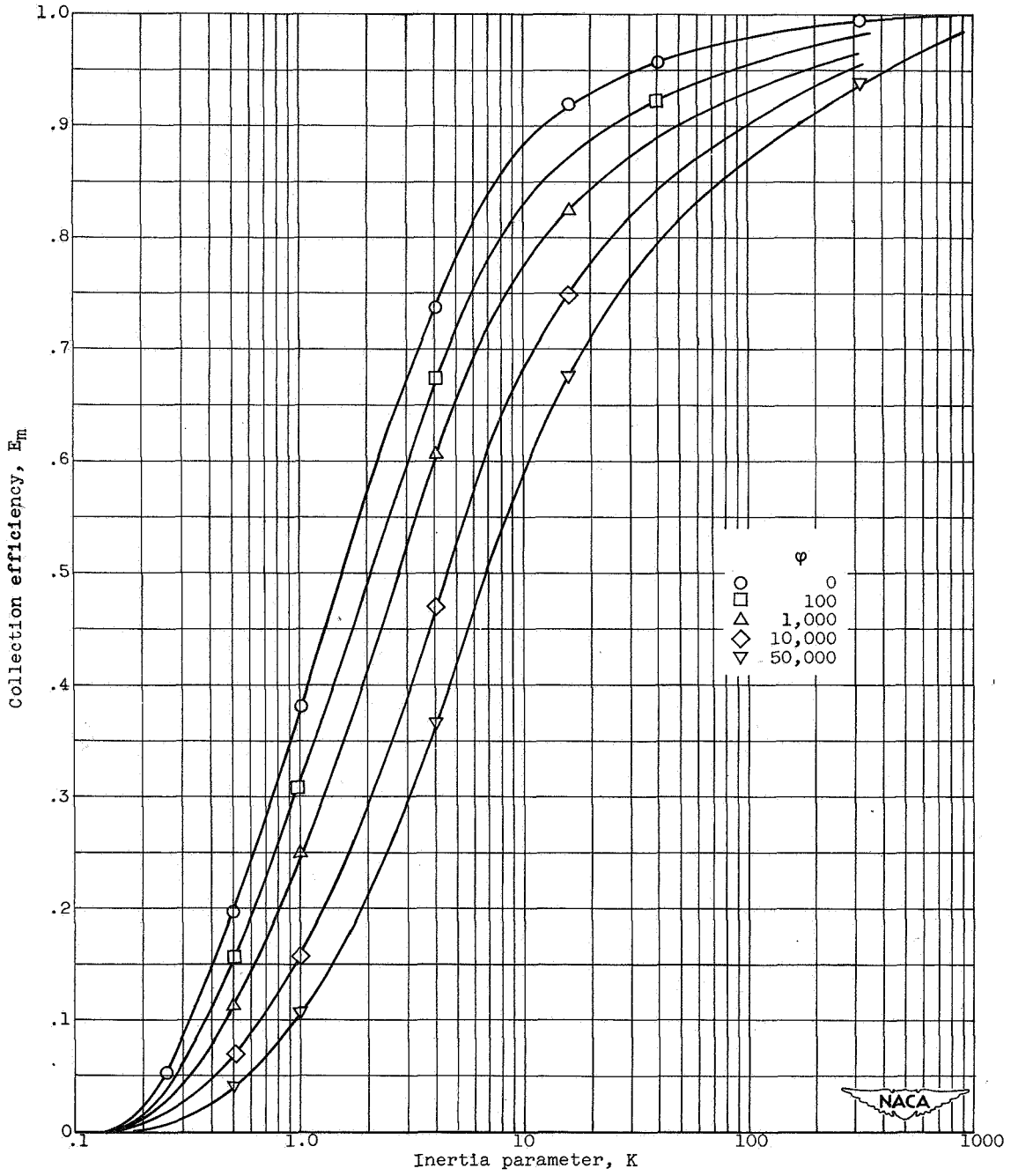

Figure 3. - Cylinder collection efficiency in compressible-air flow field at approximately flight critical Mach number.

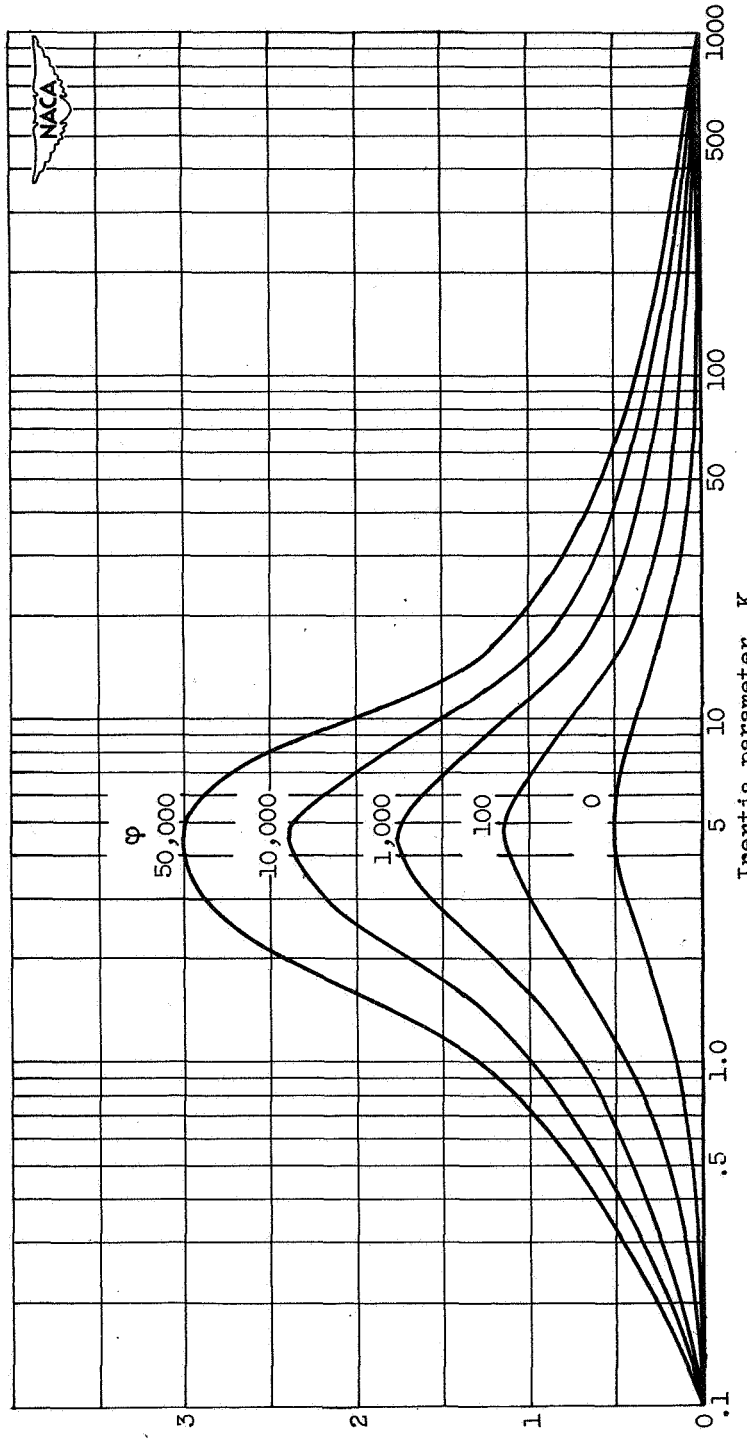

Figure 4. - Correction factor for compressibility effect.

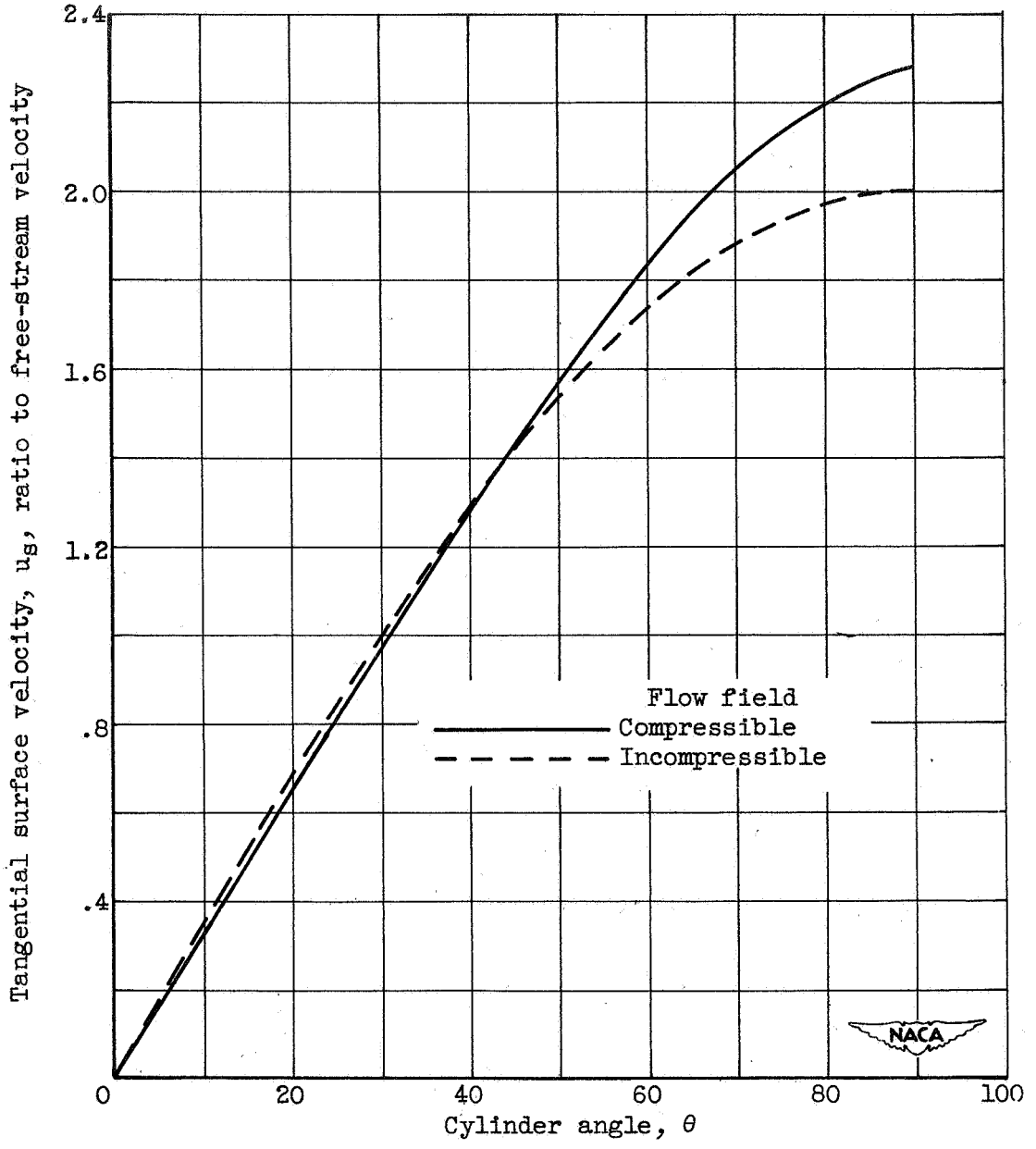

Figure 5. - Comparison of surface velocity on a cylinder between incompressible flow field and compressible-air flow field at approximately flight critical Mach number.

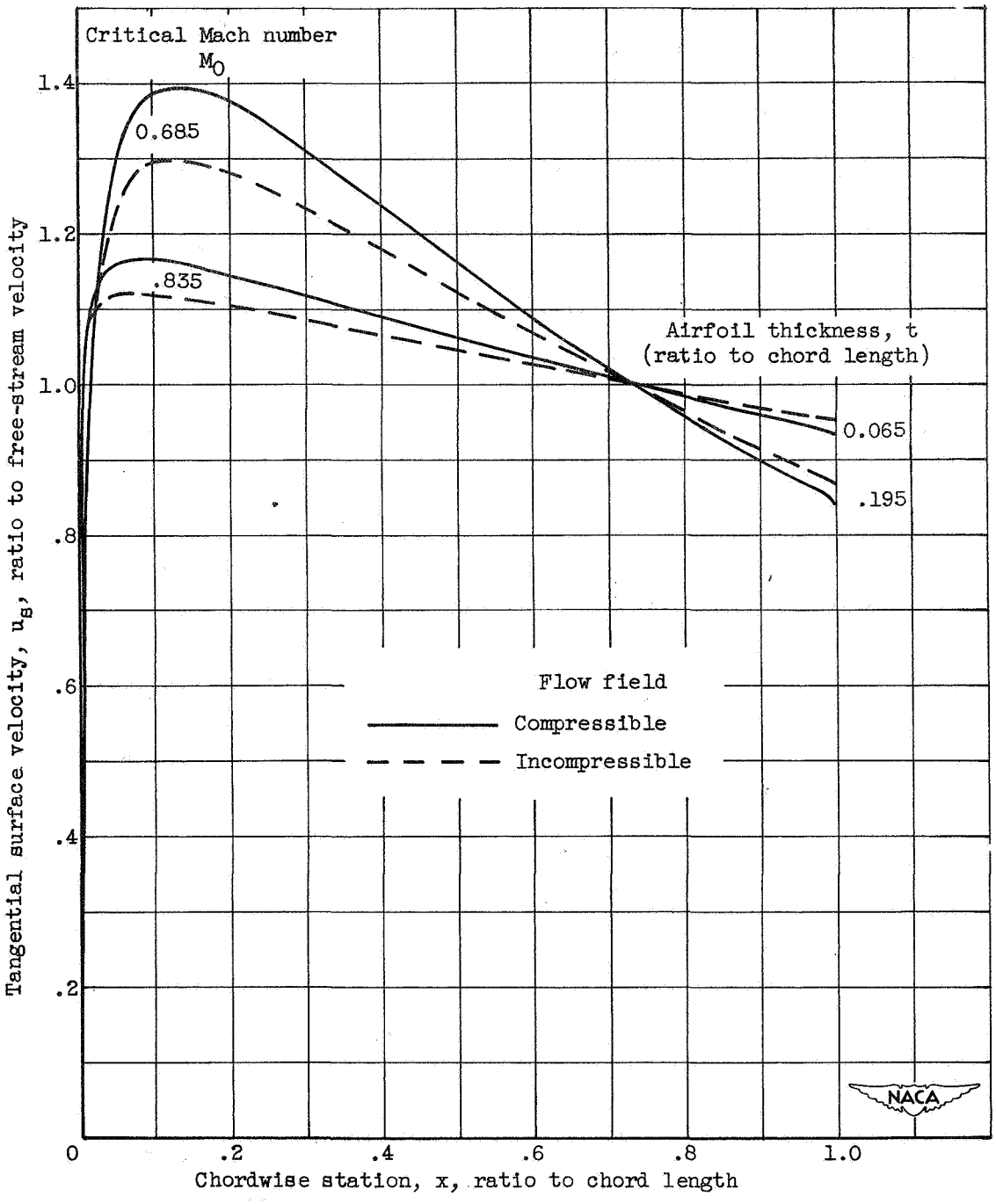

Figure 6. - Comparison of surface velocities on symmetrical Joukowski airfoils. Angle of attack, 0°.